DOI: 10.1021/ma101680g

Macromolecules
ARTICLE

Conjugated Polymer Fluorescence Probe for Intracellular Imaging of Magnetic Nanoparticles

Bin Sun,[†,∥] Min-Jie Sun,[†,‡,∥] Zhen Gu,[†,⊥] Qun-Dong Shen,*[,†] Shao-Jun Jiang,[§] Ying Xu,[‡] and Yu Wang[‡]

[†]*Department of Polymer Science & Engineering and Key Laboratory of Mesoscopic Chemistry of MOE, School of Chemistry & Chemical Engineering, Nanjing University, Nanjing 210093, China,* [‡]*Department of Pharmaceutics, China Pharmaceutical University, Nanjing, 210009, China,* [§]*Department of Pathology and Laboratory of Electron Microscopy, Jinling Hospital, Nanjing 210002, China, and* [⊥]*School of Engineering and Applied Science, University of California, Los Angeles, California 90095, United States.* [∥]*B.S. and M.-J.S. contributed equally to this work.*

Received July 26, 2010; Revised Manuscript Received November 15, 2010

ABSTRACT: Bifunctional composite nanoparticles with simultaneous response toward light excitation and external magnetic field are fabricated by electrostatic adsorption of a single layer of conjugated polyelectrolytes on the magnetic nanoparticle surfaces. Cell imaging is realized through incubation of the composite nanoparticles with human hepatoma cell Bel-7402. Both fluorescence microscopy imaging and flow cytometry analysis verify that the bifunctional nanoparticles efficiently penetrate the cell membranes. Transmission electron microscopy reveals that the nanoparticles are confined in the endosome and show clear signs of particle aggregation. The cellular uptake efficiencies of the magnetic-fluorescent nanoparticles can be enhanced greatly by a magnetic field. In vitro cell viability results indicate low cytotoxicity of the nanoparticles even after 72 h incubation. The current method of fluorescence labeling of nanomaterials by electrostatic adsorption is applicable to a variety of charged nanomaterials that exist with great diversity in chemistry and morphology, which is necessary for estimation of cell toxicity and fundamental understanding of phenomena related to the development of nanomaterial based diagnostics and therapeutics.

1. Introduction

The emerging field of nanotechnology has brought about tremendous nanoscale materials in shapes of particles, fibers, rods, disks, platelets, and tubes with unique chemical, electronic, and optical properties. Nanomaterials have recently attracted intense interests in biology and medicine, including carriers for drug and gene delivery,[1] highly sensitive and selective sensors for biological species,[2−6] in vivo targeting, imaging, and diagnostics.[7−11] Nanomaterials can couple with biomolecules through electrostatic interactions.[12] Nanomaterials have extremely small sizes, which facilitate their uptake into a wide variety of living cells. The rapid development of nanotechnology thereby offers possibilities of unintentional inhalation or ingestion of nanomaterials by living creatures and attendant health risks.[13,14] It creates a desire for more knowledge on what happens and when an organism encounters the nanomaterials, including the endocytosis and adverse effects on living cells.

For tracking the cellular uptake of nanomaterials, both fluorescence imaging and magnetic resonance imaging (MRI) are frequently used.[15] A number of fluorescent probes for cellular imaging have been built upon nanomaterials, such as small molecular organic dyes, inorganic semiconductive nanocrystals, and fluorescent protein nanocarriers.[16−22] The strategies to such hybrid nanoparticles require elaborate chemical processes, including coupling the fluorophores to nanoparticles by covalent linkages and nanoparticle encapsulation by an inorganic/organic shell of fluorophores. In this report, we present a new platform for cellular uptake and intracellular imaging of magnetic nanoparticles (MPs) using conjugated polymers as fluorescent probes. The fluorescent polymer (BtPFN) described here has a π-conjugated backbone and quaternary ammonium ions on the side chains (Figure 1a). Conjugated polymers are highly efficient at harvesting and emitting light energy, and have been explored as high-sensitivity and high-selectivity chemical/biological sensors[23−35] and fluorescence imaging agents.[36−40] On the basis of electrostatic adsorption, the conjugated polyelectrolyte coats on surface of magnetic iron oxide nanoparticles to form composite nanoparticles (MPs/BtPFN) with positively charged fluorescent shell (Figure 1b). Such organic/inorganic hybrid nanoparticles display simultaneous response toward light excitation and external magnetic fields. Therefore, one is able to directly visualize the fluorescent nanoparticles internalized by cancer cells (Figure 1c). We will demonstrate cellular uptake of the fluorescently labeled magnetic nanoparticle can be aided by the application of a magnetic field. Most importantly, the current method of fluorescence labeling of nanomaterials by electrostatic adsorption is very versatile, as it depends on oppositely charged electrostatic interactions rather than specific molecular interactions. It is applicable to a variety of charged nanomaterials that exist with great chemical diversity in the form of metals, inorganic oxides, carbons, organics, and biological molecules. The emissive color of fluorescently labeled nanoparticles is also tunable by choice of different conjugated polyelectrolytes which can span the full range of the visible spectrum (400−700 nm).[41]

*Corresponding author. Telephone: +86 25 83317807. Fax: +86 25 83317761. E-mail: qdshen@nju.edu.cn.

2. Experimental Section

2.1. Materials. 2,7-Bis(4,4,5,5-tetramethyl-1,3,2-dioxaborolan-2-yl)-9,9-bis[3′-(dimethylamino) propyl] fluorene was prepared by the method described elsewhere.[32,42] 4,7-Dibromo-2,1,3-benzothiadiazole was purchased from Hanhong Chemical Co. (Shanghai, China). Tetrakis(triphenylphosphine)palladium (0) was purchased from

 Published on Web 12/02/2010

Aldrich Chemical Co. Magnetic Fe_3O_4 nanoparticles were synthesized by common chemical coprecipitation technique of iron salts.[43] Hoechst 33342 was purchased from Sigma. 3-(4,5-Dimethylthiazol-2-yl)-2,5-diphenyltetrazolium bromide (MTT) was purchased from Amresco (Solon, OH).

2.2. Synthesis of Poly{9,9-di[3′-(dimethylethylaminonium)propyl]-2,7-fluorenyl-*alt*-4,7-(2,1,3- benzothiadiazole) dibromide} (BtPFN). 2,7-Bis(4,4,5,5-tetramethyl-1,3,2-dioxaborolan-2-yl)-9,9-bis-[3′-(dimethylamino) propyl] fluorene (502 mg, 0.853 mmol), 4,7-dibromo-2,1,3-benzothiadiazole (251 mg, 0.853 mmol), and tetrakis-(triphenylphosphine)palladium (0) (40 mg) were dissolved in a degassed mixture of toluene (25 mL) and K_2CO_3 (2 mol/L, 10 mL). The mixture was stirred at 85−90 °C for 48 h under nitrogen atmosphere. After cooling down to room temperature, the mixture was extracted with chloroform, concentrated, and the desired polymer was precipitated from acetone three times. 190 mg of the final product (BtPFN precursor) was obtained as a yellow solid (yield 48%). ^{1}H NMR (300 MHz, $CDCl_3$): 8.1−8.05 (m, 4H, aromatic rings), 8.0−7.9 (m, 4H, fluorene ring), 2.3−2.0 (m, 20H, $-NCH_3$, $-NCH_2$, $-CH_2-$fluorene), 1.15−1.05 (m, 4H, $-CCH_2C-$). ^{13}C NMR (75 MHz, $CDCl_3$): 154.26, 151.04, 140.87, 136.60, 133.44, 128.47, 127.94, 123.97, 120.13, 59.87, 55.06, 45.31, 37.71, 22.18. See Figure 2 for the reaction scheme.

A 250 mL flask with a magnetic stirring bar was charged with BtPFN precursor (100 mg, 0.214 mmol) dissolved in THF (80 mL) and DMSO (20 mL). Bromoethane (2.9 g, 27 mmol) was then added. The reaction mixture was stirred at 50 °C for 5 days. Then the precipitate was collected by centrifugation and washed with acetone. After being dried under vacuum for 24 h, 116 mg of the final product (BtPFN) was obtained (yield 79%). ^{1}H NMR (300 MHz, DMSO-d_6): 8.4−8.0 (m, 8H, aromatic rings), 3.3−3.1 (m, 8H, $-NCH_2$), 2.9 (s, 12H, -NCH_3), 2.6 (m, 4H, fluorene$-CH_2$), 2.4−2.1 (m, unquaternized $-NCH_{x=2-3}$), 1.6−1.3 (m, 4H, $-CCH_2C-$), 1.1−1.0 (m, 6H, $-CCH_3$). ^{13}C NMR (75 MHz, DMSO-d_6): 154.00, 150.18, 140.37, 136.77, 132.84, 129.55, 129.18, 124.93, 121.37, 62.79, 58.91, 57.10, 54.40, 49.86, 42.54, 35.31, 18.12, 8.10. A quaternization degree of about 85% was estimated.

2.3. Preparation of Magnetic−Fluorescent Nanoparticles by Electrostatic Assembly. Magnetic iron oxide nanoparticles were dispersed in an aqueous solution containing NaCl (20 mmol/L) and tris(hydroxymethyl)aminomethane (Tris, 20 mmol/L, pH = 8.90). The solution was added to a BtPFN solution (1 mmol/L) and kept for 30 min under ultrasonic agitation for thorough adsorption. The magnetic-fluorescent nanoparticles (MPs/BtPFN) were purified three times by magnetic separation and washing.

2.4. Cell Internalization of Magnetic−Fluorescent Nanoparticles. Bel-7402 cells were seeded onto coverslips in 6-well plate at 1×10^5 cells per well. The plate was washed with phosphate buffered saline (PBS). Then, the magnetic-fluorescent nanoparticles were added into the medium. After 4 h to 72 h incubation at 37 °C, the medium in each well was removed and the wells were washed twice with PBS. For magnetic field induced cell uptake, cells (Bel-7402) were seeded in two 24-well plate at 1×10^5 cells per well. The plate was washed with phosphate buffered saline (PBS). Then, the fluorescent nanoparticles were added into the medium. One of the plate was put on the neodymium magnets (15 × 5 mm column, distance between cell plate and magnet was about 3 mm). After 0.5−2 h incubation at 37 °C, the medium in each well was removed and the wells were washed twice with PBS. Cells were washed with PBS and incubated with trypsinogen (0.25% trypsin) to detach from the plates. After centrifugation, cells were washed with PBS twice. Then fluorescence was analyzed using a BD FACSCalibur flow cytometer (Becton−Dickinson).

2.5. Instrumentation and Measurements. ^{1}H NMR and ^{13}C NMR spectra were collected on a Bruker DRX-300 spectrometer. Electrophoretic mobility of the bare and surface-coated magnetic nanoparticles was measured using a ζ potential analyzer

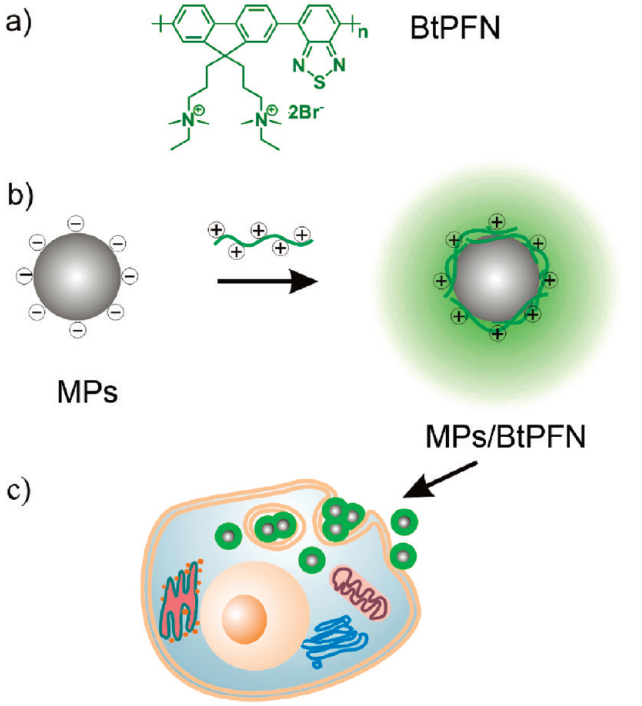

Figure 1. (a) Chemical structure of the conjugated polymer (BtPFN) described in the text. (b) Electrostatic adsorption of BtPFN on surfaces of oppositely charged magnetic nanoparticles to afford magnetic-fluorescent nanoparticles, which are then internalized by cancer cells (c).

(BI-9000AT and Zetaplus, Brookhaven Instruments Corporation). Magnetic measurements were performed at Quantum Design MPMS-XL7 SQUID magnetometer. The iron content in the nanoparticles was determined with an atomic absorption spectrophotometer (Varian 240FS). Electron absorption spectra were measured on a Shimadzu UV-3100 spectrophotometer. Fluorescence spectra were measured on SLM 48000 DSCF.AB2 spectrometer.

Confocal laser scanning microscopy was performed in a Leica TCS SP5 confocal laser scanning microscope at excitation wavelength of 435/405 nm. The cells were fixed with 4% of paraformaldehyde solution for 15 min, and washed three times with PBS after removal of the fixing solution. Flow cytometry analysis was performed by a BD FACSCalibur flow cytometer (Becton-Dickinson). Sheath fluid was Coulter Isoton III diluent (Beckman-Coulter).

The fine structure of cells was examined in a Jeol JEM-1011 (Jeol Ltd., Tokyo, Japan) transmission electron microscope. Bel-7402 cells incubated with MPs/BtPFN were prefixed at 4 °C overnight with 2.5% glutaraldehyde in PBS. The cells were rinsed with PBS three times. Next, the cells were postfixed for 45 min with 1% OsO_4 dissolved in PBS. After removal of the osmium by immersion in water for 10 min, the cells were gradually dehydrated and then were embedded in epoxy resin (EPON 812, SPI Supplies, West Chester, PA) by polymerization for 24 h at 60 °C. Ultrathin sections of the embedded cells were stained with uranyl acetate/lead citrate.

The cell viability was determined by a microplate reader (Thermo Electron Corporation). 200 μL (1×10^5 cells per microliter) of cells were transferred to 96-well plate. Then, the medium was replaced with 200 μL of medium containing the nanoparticles with various concentrations. One row of the 96-well plates was used as control. After 24 or 72 h incubation, the medium in each well was removed and the wells were washed three times using PBS. 20 μL of MTT and 180 μL of medium were then added to the wells. After incubation for 4 h, the solution was removed, leaving the precipitate. Two hundred

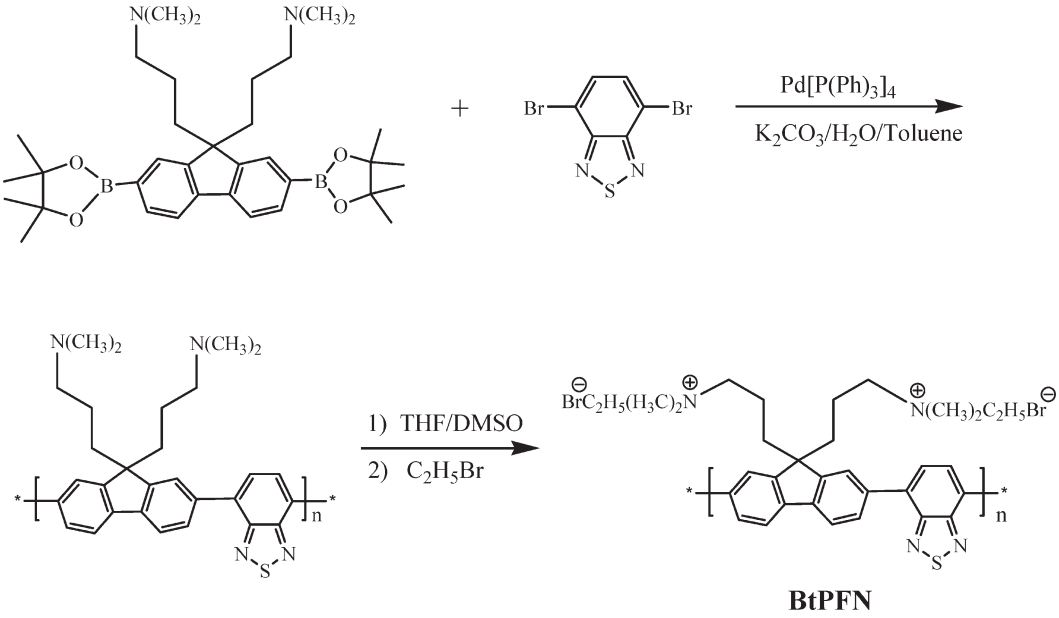

Figure 2. Synthetic routes to BtPFN by Suzuki coupling.

microliters of DMSO was then added to the wells before the plate was observed using a microplate reader.

3. Results and Discussion

3.1. Photophysical Properties of the Conjugated Polymer. Cationic polyfluorenes and their alternating copolymers with benzene units are high-efficiency blue-emitting materials widely used in the scheme of biosensors. Earlier works on alternating copolymers of fluorene with heterocyclic compounds indicates that electron-deficient monomers are effective in shifting the emission band of polyfluorenes to longer wavelength, which is highly desirable for multicolor fluorescence sensor and imaging systems.[32,42,43] Here we use a cationic benzothiadiazole−fluorene alternating copolymer, which is abbreviated as BtPFN (Figure 1a). Fluorene monomer units with cationic alkyl side chains render water-solubility without significantly altering the electronic structure of the conjugated backbone. The electron absorption and fluorescence emission spectra of a diluted BtPFN aqueous solution (10 μmol/L) are shown in Figure 3. The cationic conjugated polymer has two well-separated absorption bands at 319 and 437 nm, which arise from the absorption of light by the π-electron system of the conjugated backbone.[44,45] The introduction of benzothiadiazole units to polyfluorene chains leads to significant red-shift of excitation wavelength. Therefore, live biological cells can be optically imaged using a blue (wavelength $>$ 400 nm) excitation light to minimize ultraviolet-induced photodamage. Once BtPFN in water is photoexcited, it returns to ground state by emission of structure-less yellowish-green light with a maximum wavelength of 552 nm, and the emission spectrum is independent of excitation wavelength.

3.2. Fluorescent−Magnetic Nanoparticles. Fluorescent labeling of magnetic Fe_3O_4 nanoparticles (MPs) is carried out by electrostatic adsorption technique (Figure 1b). The as-prepared magnetite nanoparticles in Tris buffer (pH = 8.90) are negatively charged with a ζ potential of −44 mV, verifying particle stability in aqueous suspensions. Dynamic light scattering affords hydrodynamic diameters of the nanoparticles in the range of 30−50 nm. The magnetization curve of the nanoparticles obtained by cycling the field between −30 and +30 kOe shows no hysteresis (Figure 4a), indicating the iron oxide nanoparticles are superparamagnetic.

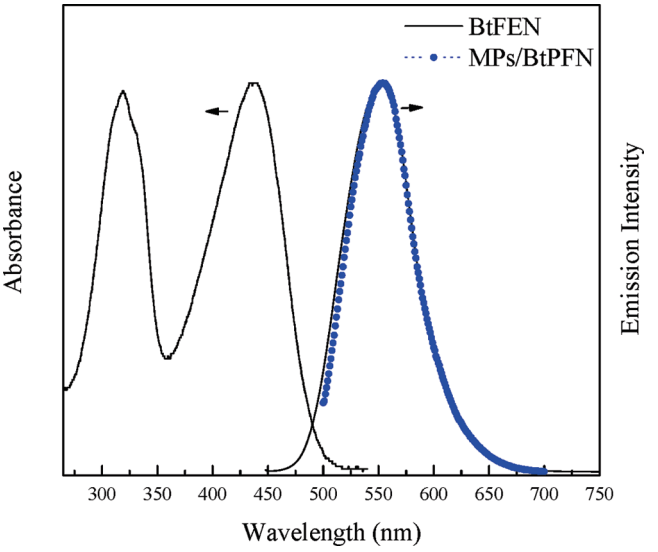

Figure 3. Electron absorption and photoluminescence spectra (excitation wavelength of 437 nm) of BtPFN in aqueous solution. Also shown is the emission spectrum of magnetic nanoparticles fluorescently labeled by BtPFN.

In the presence of BtPFN, ζ potentials of the magnetic nanoparticles change dramatically from negative to positive values at polymer concentration higher than 10 μmol/L. It is evidence of strong interaction between the cationic conjugated polyelectrolyte and the oppositely charged magnetic nanoparticle. Zeta potential of the magnetic nanoparticles reaches a value of +36 mV at saturated adsorption of the cationic polyelectrolyte (1 mmol/L). High ζ potential value confers stability of positively charged MPs/BtPFN nanoparticles, i.e. resistance of such colloidal dispersions to coagulate or flocculate. As is shown in Figure 4b, MPs/BtPFN nanoparticles display response toward permanent magnets. A prominent separation of the nanoparticles from the solution is observed. Such fluorescent nanoparticles can thereby be purified by repeated magnetic separation/wash/redispersion

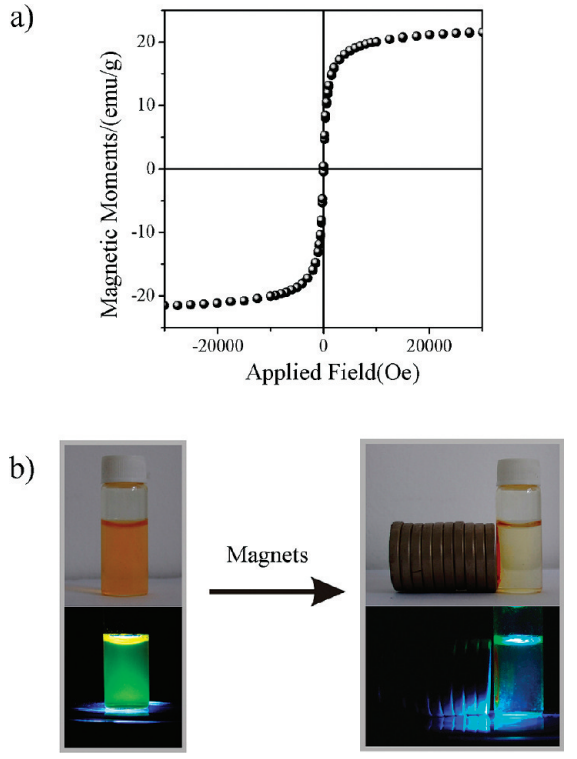

Figure 4. (a) Magnetization hysteresis loop of the nanoparticles measured at 300 K. (b) Photographs show an aqueous dispersion of fluorescently labeled nanoparticles and their responses to magnetic fields (excitation wavelength of 450 nm).

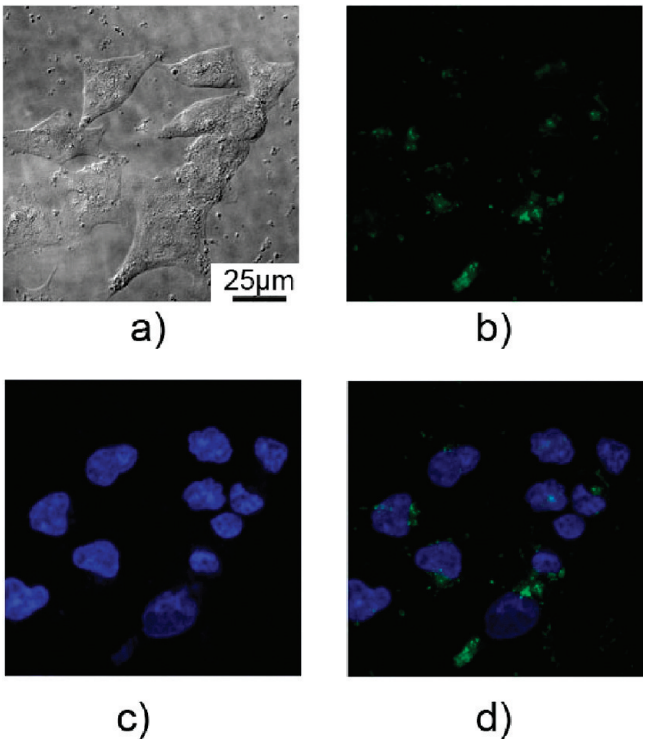

Figure 5. CLSM images of Bel-7402 cells incubated with MPs/BtPFN (green color) for 4 h at 37 °C, whereas cell nuclei are stained by Hoechst 33342 dye (blue color). (a) Bright-field image. (b–d) Fluorescence images of the green (b) and blue (c) channeles, and a merged image (d).

cycles to remove the excess conjugated polyelectrolytes free from electrostatic adsorption. Iron element in the stock aqueous solution of MPs/BtPFN nanoparticles is found at a concentration of 0.27 mg/mL by atomic absorption spectrophotometer. Emission spectrum of MPs/BtPFN nanoparticles (Figure 3) is very similar to that of the cationic conjugated polymer, suggesting that the magnetic nanoparticles scarcely interfere with emission from BtPFN.

3.3. Uptake of Fluorescent–Magnetic Nanoparticles by Live Cancer Cells. To demonstrate that magnetic nanoparticles fluorescently labeled by conjugated polyelectrolytes can be effectively internalized into human hepatoma carcinoma cells (Bel-7402), confocal laser scanning microscopy (CLSM) is performed to examine the cells. After the incubation of Bel-7402 cells with MPs/BtPFN for 4 h at 37 °C, a blue organic dye (Hoechst 33342) is added to stain cell nuclei. The cells are fixed by paraformaldehyde solution for fluorescence imaging studies.

The CLSM images are shown in Figure 5. Bright-field image obtained by differential interference contrast (DIC) technique provides good contrast of morphological features in Bel-7402 cells (Figure 5a). Fluorescence images collected for two channels show characteristic green and blue fluorescence from BtPFN and Hoechst 33342, respectively (Figure 5b,c). The green fluorescent part therefore resembles the distribution of MPs/BtPFN nanoparticles. Separate green and blue channel images are merged to reveal that there is no colocalization of the two fluorophores (Figure 5d). Since Hoechst 33342 has very high affinity for DNA in the cell nuclei, the results indicate most MPs/BtPFN nanoparticles are clearly in the cytoplasm, whereas a few of them migrate to the region very close to outer nuclear membranes of the cells. Previous reports have substantially supported that nanomaterials can be ingested by live cells.[13,14,46]

The representative fluorescence images do not specify the exact location of MPs/BtPFN nanoparticles in the cytoplasm. Therefore, transmission electron microscope (TEM) examinations are carried out to provide a high spatial resolution of the nanoparticles in live cells. Figure 6 shows typical TEM images of Bel-7402 cells after incubation with MPs/BtPFN for 4 h at 37 °C. The nanoparticles are readily taken up by the cells and are confined to the endosomes (Figure 6a). The nanoparticles in the endocytic vesicles show clear signs of particle aggregation (Figure 6b). Agglomeration of the nanoparticles may be explained by nonspecific interaction between individual nanoparticles. The pathways of cellular internalization of MPs/BtPFN and targeting subcellular structures are needed to be addressed. Endocytosis by cells embraces several routes of internalization. Figure 6c clearly shows adhesion of the nanoparticles to the cell surface. It suggests the positively charged nanoparticles undergo interactions with substances (for example, negatively charged proteoglycans) located in the extracellular matrix. Once the nanoparticles adhere to a cell membrane, the lipid membrane is stimulated to form a small pocket locally around the nanoparticles and enclose them gradually, leading to internalization of the nanoparticles in the vesicle (the endosomes).[47,48] TEM image of as-prepared MPs/BtPFN is also displayed (Figure 6d) to provide a better comparison with that in the cancer cell. Both images reveal that the nanoparticles are in the same geometry and particle size.

In view of electrostatic or hydrophobic characteristics, the cationic conjugated polymers coated on the nanoparticles are prone to interactions with proteins or other biomolecules throughout the cell internalization experiments. Combined with confocal fluorescence microscopy analysis, the BtPFN coating is quite firmly packed on the nanoparticle surface.

For live cell nanoparticle tracking, surface plasmon resonance of metal nanoparticles, magnetic resonance imaging,

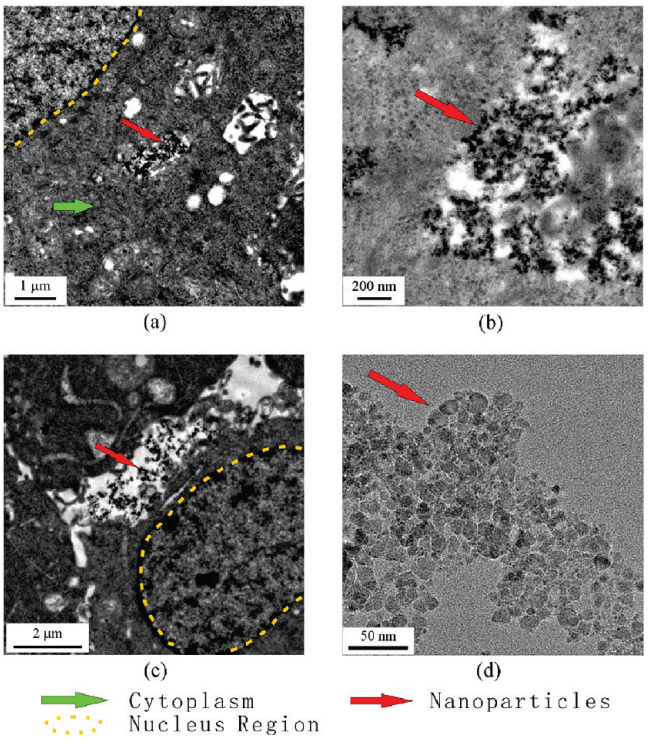

Figure 6. TEM images (a−c) demonstrate internalization of MPs/BtPFN nanoparticles into Bel-7402 cells after 4 h of incubation. The nanoparticles are visible as black dots. Also shown is the morphology of as-prepared MPs/BtPFN nanoparticles (d).

and electron microscopy have proven to be extraordinarily useful, while these methods are time-consuming and not widely applicable to numerous nanomaterials with considerable interest. Fluorescence labeling of nanomaterials by conjugated polymers enables optical imaging of cellular uptake of the nanomaterials with diverse morphology and composition. Moreover it is capable of rapid (up to thousands of cells per second) single-cell fluorescence analysis by flow cytometry (FCM) technique. Figure 7 quantifies fluorescent intensity for multiple cell populations by a flow cytometer. Both Bel-7402 cells cultured in the absence (control sample) and presence of MPs/BtPFN (5.4 μg/mL) are measured. The signals are monitored at 575 nm (FL2), close to fluorescence emission maximum of BtPFN. The control sample shows cellular autofluorescence of very low emission intensity. The observed significant increase in cell fluorescence by one or 2 orders of magnitude proves cellular uptake of conjugated polymer-labeled magnetic nanoparticles. Almost all of the Bel-7402 cells are found to contain MPs/BtPFN. The intensity distribution is broad, indicating the number of fluorescent nanoparticles taken up by live cells during incubation varies over a wide range. The variables appearing to be critical for cellular uptake efficiency of the nanoparticles include the size of the nanoparticle, the charge of the nanoparticle surface, the cell type, and so on. It has been extensively approved that internalization capability of nanoparticles can be considerably changed by simply altering one of these variables. When the nanoparticles translocate across cell membranes, the difference of uptake efficiency is dependent on such factors as conjugation of nanoparticles to surface receptors/proteins or proteoglycans in the extracellular matrix and nonspecific interactions with the lipid membrane.

3.4. Magnetic-Field Aided Cell Uptake of MPs/BtPFN Nanoparticles. Biological application of magnetic nanomaterials

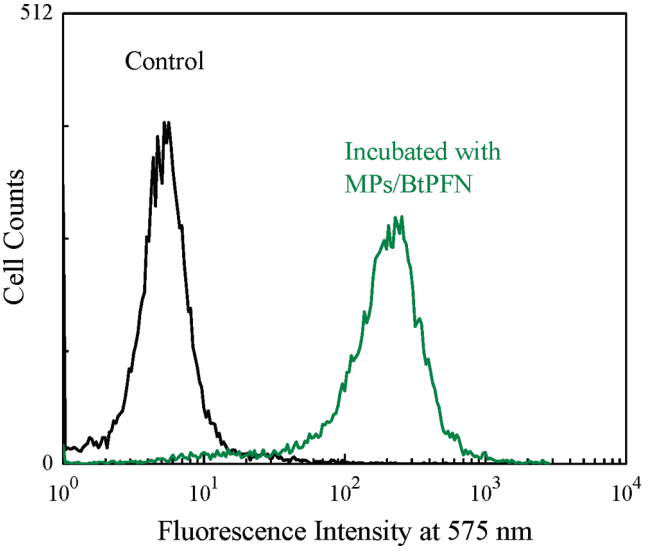

Figure 7. Flow cytometry results. The excitation wavelength is 488 nm. From left to right: Bel-7402 (control) and the cells incubated with MPs/BtPFN (5.4 μg/mL).

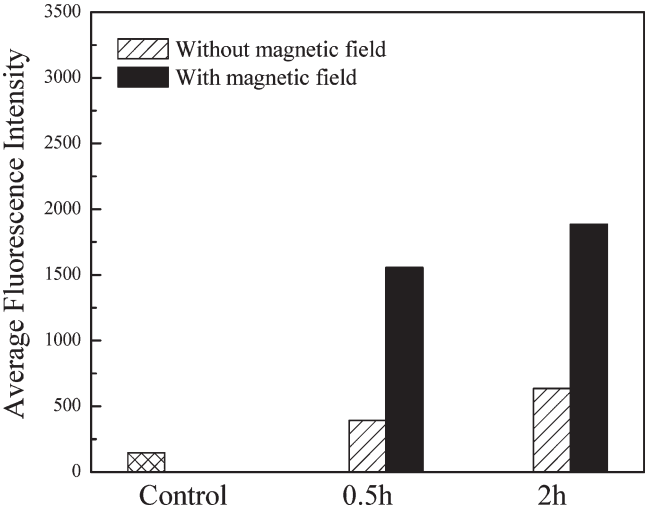

Figure 8. Bel-7402 cells incubated with MPs/BtPFN (2.7 μg/mL) for 0.5−2 h, with or without assistance of magnetic field.

for targeted drug delivery, magnetic separation of cells, magnetic resonance contrast enhancement, and magnetically induced hyperthermia to kill tumor cells have been well established. Inspired by these results, we further interrogate the magnetic response ability of MPs/BtPFN nanoparticles toward the cellular uptake efficiency, which is determined by the flow cytometry analysis. As is shown in Figure 8, in the absence of a magnetic inducement by magnets, the uptake of the fluorescent polymer-labeled magnetic nanoparticles with a lower concentration (2.7 μg/mL) is insignificant. In contrast, with the aid of magnetic field, uptake efficiency of MPs/BtPFN dramatically increases. For the sample with a 2 h continuous treatment by magnetic field, a 3-fold enhancement of the average cellular fluorescence intensity can be observed. The notable enrichment of cellular uptake effect by MPs/BtPFN upon the magnetic field treatment is useful for on demand imaging or physical therapy, where stimuli responsive action or targeting enrichment is needed.

MPs/BtPFN nanoparticles have positive surface charges and should be adsorbed to lipid membrane surfaces. The

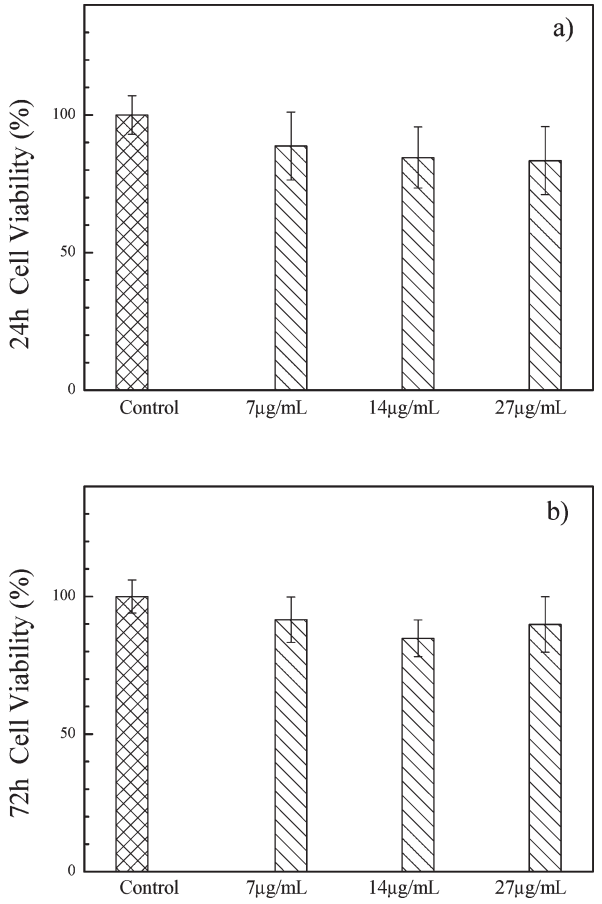

Figure 9. In vitro viability of Bel-7402 cells treated with MPs/BtPFN (7−27 μg/mL) for (a) 24 h and (b) 72 h incubation.

subsequent internalization of MPs/BtPFN requires energies for induction of membrane curvature or formation of endosome. Thereby, the endocytosis processes are time-dependent. Internalization is greatly enhanced by magnetic forces, which do not alter the uptake mechanism but accelerate sedimentation of the nanoparticles on the cell surface, and provide extra energy for internalization of the nanoparticles.

3.5. Effect of Magneto-Optical Nanoparticles on Cancer Cells in the Extended Incubation Period. Long-term effects of the internalized MPs/BtPFN, as an alternative candidate for biological application, on live cells should be assessed. In vitro cell viability results obtained by MTT colorimetric assay are presented in Figure 9a. After a 24 h exposure, low cytotoxicity in Bel-7402 cells is found for MPs/BtPFN. Cell viabilities have rather weak concentration dependence over the whole concentration range from 7 to 27 μg/mL. It is needed to emphasize that the concentration of the nanoparticles used in fluorescence imaging is 2.7 μg/mL, only one tenth of that in cytotoxicity evaluation. Biocompatibility of the live cells incubated with the magnetic-fluorescent nanoparticles for 72 h further displays low cytotoxicity of the nanoparticles with a concentration up to 27 μg/mL (Figure 9b).

It is of importance to find out the intracellular fate of MPs/BtPFN nanoparticles. After incubation with MPs/BtPFN for 48 h at 37 °C, Bel-7402 cells (Figure 10a) are selectively stained with Hoechst 33342. The confocal fluorescence image obtained at *xy*-plane parallel to the substrate clearly shows the nanoparticles are still visible in cytoplasm of Bel-7402 cells, supporting long-term stability of the nanoparticles. Colocalization of blue and green signals is found in the

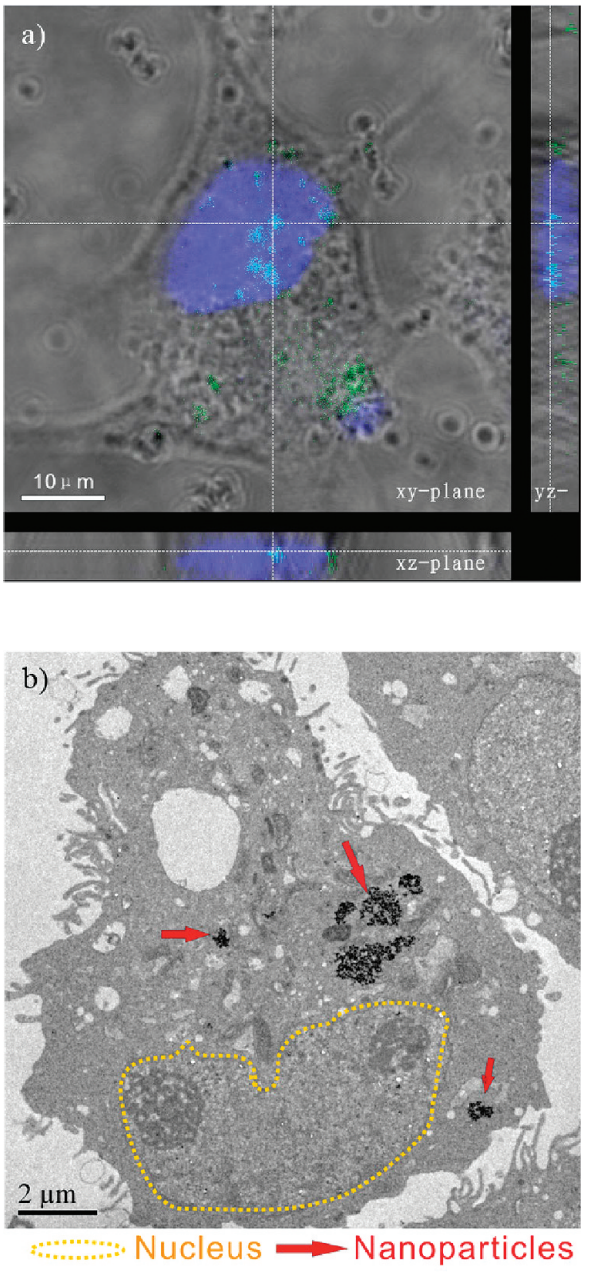

Figure 10. (a) Confocal optical and (b) TEM images of Bel-7402 cells incubated with MPs/BtPFN (green color) for 48 h at 37 °C. The cell nuclei are stained by Hoechst 33342 (blue color).

cell nuclear region. Moreover, images of *xz*-plane and *yz*-plane perpendicular to the substrate are also obtained by graphical reconstruction from a series of *z*-scans, implying that MPs/BtPFN may penetrate into the cell nucleus. While cells indeed tend to deal with intruding nanoparticles by confining them to the endosome, it is hard to find out what happens to the magnetic-fluorescent nanoparticles once they are inside the cell and why they target specific sites, such as the nucleus. It also seems cells have difficulty excluding nanoparticles intruders.

TEM image (Figure 10b) shows that most of the nanoparticles stay in the cytoplasm, which is consistent with the results from fluorescence imaging. However, there are only few black dots in the nuclear region. In contrast, green fluorescence signal from the conjugated polymers is discerned within the cell nuclear region. In view of effective transportation diameter of the nuclear pore (~9 nm), only

few percentage of the magnetic nanoparticles with extremely small size would penetrate into the nuclei by passive diffusion, as confirmed by TEM observation. Other molecular mechanisms may permit nuclear transport of the colloidal particles with a diameter at least 20 nm.[49] However, it seems that MPs/BtPFN does not benefit from such transport mechanisms. Fluorescent signal in the nucleus, thus, may indicate that MPs/BtPFN migrates to the region immediately adjacent to the nuclear pores. Another possibility is that conjugated polymers may penetrate into nuclei, while leave the magnetic nanoparticles behind.

4. Conclusions

In summary, we demonstrate the feasibility of fluorescence labeling of magnetic nanoparticles by electrostatic adsorption of conjugated polyelectrolytes. Facile preparation, effective cell-penetration, long-term stability, and low cytotoxicity render this strategy as a good candidate for tracking nanoparticles in cell biological study and clinical diagnostics. Composite nanoparticles encapsulated by conjugated polyelectrolytes can be used as robust fluorescent probes in cell imaging, and if optimized, as multicolor probes to detect interactions of tremendous nanoparticles with living cells. Moreover, given merits of instantaneous response upon the magnetic field stimuli, this hybrid nanoparticles can be further developed as in vivo imaging agents for high-sensitivity, high-resolution detection and cancer-cell destruction (tumor therapy) in alternating magnetic field, where both of optical imaging and magnetic resonance imaging are essential.

Acknowledgment. This work is supported by the National Natural Science Foundation of China under Contract No. 20774040. The authors thank Professor Yin Lu at Nanjing University of Traditional Chinese Medicine for providing human hepatoma carcinoma cells used in this study.

References and Notes

(1) Allen, T. M.; Cullis, P. R. *Science* **2004**, *303*, 1818.
(2) Chan, W. C. W.; Nie, S. M. *Science* **1998**, *281*, 2016.
(3) Cui, Y.; Wei, Q. Q.; Park, H. K.; Lieber, C. M. *Science* **2001**, *293*, 1289.
(4) Haes, A. J.; Van Duyne, R. P. *J. Am. Chem. Soc.* **2002**, *124*, 10596.
(5) Nam, J. M.; Thaxton, C. S.; Mirkin, C. A. *Science* **2003**, *301*, 1884.
(6) Wong, S. S.; Joselevich, E.; Woolley, A. T.; Cheung, C. L.; Lieber, C. M. *Nature* **1998**, *394*, 52.
(7) Bruchez, M.; Moronne, M.; Gin, P.; Weiss, S.; Alivisatos, A. P. *Science* **1998**, *281*, 2013.
(8) Gao, X. H.; Cui, Y. Y.; Levenson, R. M.; Chung, L. W. K.; Nie, S. M. *Nat. Biotechnol.* **2004**, *22*, 969.
(9) Li, Z. F.; Ruckenstein, E. *Nano Lett.* **2004**, *4*, 1463.
(10) Michalet, X.; Pinaud, F. F.; Bentolila, L. A.; Tsay, J. M.; Doose, S.; Li, J. J.; Sundaresan, G.; Wu, A. M.; Gambhir, S. S.; Weiss, S. *Science* **2005**, *307*, 538.
(11) Rosi, N. L.; Mirkin, C. A. *Chem. Rev.* **2005**, *105*, 1547.
(12) Niemeyer, C. M. *Angew. Chem., Int. Ed.* **2001**, *40*, 4128.
(13) Oberdorster, G.; Oberdorster, E.; Oberdorster, J. *Environ. Health Persp.* **2005**, *113*, 823.
(14) Service, R. F. *Science* **2008**, *321*, 1036.
(15) Mailander, V.; Landfester, K. *Biomacromolecules* **2009**, *10*, 2379.
(16) Gao, J. H.; Gu, H. W.; Xu, B. *Acc. Chem. Res.* **2009**, *42*, 1097.
(17) Hu, S.-H.; Gao, X. *J. Am. Chem. Soc.* **2010**, *132*, 7234.
(18) Gao, J. H.; Zhang, W.; Huang, P. B.; Zhang, B.; Zhang, X. X.; Xu, B. *J. Am. Chem. Soc.* **2008**, *130*, 3710.
(19) Beaune, G.; Menager, C.; Cabuil, V. *J. Phys. Chem. B* **2008**, *112*, 7424.
(20) Gu, H. W.; Zheng, R. K.; Zhang, X. X.; Xu, B. *J. Am. Chem. Soc.* **2004**, *126*, 5664.
(21) Yan, M.; Du, J. J.; Gu, Z.; Liang, M.; Hu, Y. F.; Zhang, W. J.; Priceman, S.; Wu, L. L.; Zhou, Z. H.; Liu, Z.; Segura, T.; Tang, Y.; Lu, Y. F. *Nat. Nanotechnol.* **2010**, *5*, 48.
(22) Yi, D. K.; Selvan, S. T.; Lee, S. S.; Papaefthymiou, G. C.; Kundaliya, D.; Ying, J. Y. *J. Am. Chem. Soc.* **2005**, *127*, 4990.
(23) Jiang, H.; Taranekar, P.; Reynolds, J. R.; Schanze, K. S. *Angew. Chem., Int. Ed.* **2009**, *48*, 4300.
(24) Thomas, S. W.; Joly, G. D.; Swager, T. M. *Chem. Rev.* **2007**, *107*, 1339.
(25) Gu, Z.; Chen, X.-Y.; Shen, Q.-D.; Ge, H.-X.; Xu, H.-H. *Polymer* **2010**, *51*, 902.
(26) Gu, Z.; Bao, Y. J.; Zhang, Y.; Wang, M.; Shen, Q. D. *Macromolecules* **2006**, *39*, 3125.
(27) Chen, L. H.; McBranch, D. W.; Wang, H. L.; Helgeson, R.; Wudl, F.; Whitten, D. G. *Proc. Natl. Acad. Sci. U.S.A.* **1999**, *96*, 12287.
(28) Gaylord, B. S.; Heeger, A. J.; Bazan, G. C. *Proc. Natl. Acad. Sci. U. S.A.* **2002**, *99*, 10954.
(29) He, F.; Tang, Y. L.; Wang, S.; Li, Y. L.; Zhu, D. B. *J. Am. Chem. Soc.* **2005**, *127*, 12343.
(30) Tang, Y. L.; Feng, F. D.; He, F.; Wang, S.; Li, Y. L.; Zhu, D. B. *J. Am. Chem. Soc.* **2006**, *128*, 14972.
(31) Feng, X.; Duan, X.; Liu, L.; Feng, F.; Wang, S.; Li, Y.; Zhu, D. *Angew. Chem., Int. Ed.* **2009**, *48*, 5316.
(32) Liu, B.; Bazan, G. C. *Proc. Natl. Acad. Sci. U.S.A.* **2005**, *102*, 589.
(33) An, L.; Liu, L.; Wang, S.; Bazan, G. C. *Angew. Chem., Int. Ed.* **2009**, *48*, 4372.
(34) Pinto, M. R.; Schanze, K. S. *Proc. Natl. Acad. Sci. U.S.A.* **2004**, *101*, 7505.
(35) Xia, F.; Zuo, X. L.; Yang, R. Q.; Xiao, Y.; Kang, D.; Vallee-Belisle, A.; Gong, X.; Heeger, A. J.; Plaxco, K. W. *J. Am. Chem. Soc.* **2010**, *132*, 1252.
(36) Feng, X. L.; Tang, Y. L.; Duan, X. R.; Liu, L. B.; Wang, S. *J. Mater. Chem.* **2010**, *20*, 1312.
(37) McRae, R. L.; Phillips, R. L.; Kim, I. B.; Bunz, U. H. F.; Fahrni, C. J. *J. Am. Chem. Soc.* **2008**, *130*, 7851.
(38) Moon, J. H.; McDaniel, W.; MacLean, P.; Hancock, L. E. *Angew. Chem., Int. Ed.* **2007**, *46*, 8223.
(39) Pu, K.-Y.; Li, K.; Shi, J.; Liu, B. *Chem. Mater.* **2009**, *21*, 3816.
(40) Wu, C.; Bull, B.; Szymanski, C.; Christensen, K.; McNeill, J. *ACS Nano* **2008**, *2*, 2415.
(41) Zhao, X.; Pinto, M. R.; Hardison, L. M.; Mwaura, J.; Muller, J.; Jiang, H.; Witker, D.; Kleiman, V. D.; Reynolds, J. R.; Schanze, K. S. *Macromolecules* **2006**, *39*, 6355.
(42) Pu, K.-Y.; Liu, B. *Adv. Funct. Mater.* **2009**, *19*, 277.
(43) Sun, B.; Zhang, Y.; Gu, K.-J.; Shen, Q.-D.; Yang, Y.; Song, H. *Langmuir* **2009**, *25*, 5969.
(44) Stevens, M. A.; Silva, C.; Russell, D. M.; Friend, R. H. *Phys. Rev. B* **2001**, *63*.
(45) Cornil, J.; Gueli, I.; Dkhissi, A.; Sancho-Garcia, J. C.; Hennebicq, E.; Calbert, J. P.; Lemaur, V.; Beljonne, D.; Bredas, J. L. *J. Chem. Phys.* **2003**, *118*, 6615.
(46) Magrez, A.; Kasas, S.; Salicio, V.; Pasquier, N.; Seo, J. W.; Celio, M.; Catsicas, S.; Schwaller, B.; Forro, L. *Nano Lett.* **2006**, *6*, 1121.
(47) Pelkmans, L.; Burli, T.; Zerial, M.; Helenius, A. *Cell* **2004**, *118*, 767.
(48) Nativo, P.; Prior, I. A.; Brust, M. *ACS Nano* **2008**, *2*, 1639.
(49) Dworetzky, S. I.; Feldherr, C. M. *J. Cell Biol.* **1988**, *106*, 575.